



## Design, synthesis, molecular docking, and *in vitro* studies of 2-mercaptoquinazolin-4(3*H*)-ones as potential anti-breast cancer agents

Manal A. Alossaimi<sup>a,\*</sup>, Yassine Riadi<sup>a</sup>, Ghaida N. Alnuwaybit<sup>a</sup>, Shadab Md<sup>b</sup>,  
Huda Mohammed Alkreathy<sup>c</sup>, Engy Elekhrawy<sup>d</sup>, Mohammed H. Geesi<sup>e</sup>, Safar M. Alqahtani<sup>a</sup>,  
Obaid Afzal<sup>a</sup>

<sup>a</sup> Department of Pharmaceutical Chemistry, College of Pharmacy, Prince Sattam bin Abdulaziz University, Al-Kharj 11942, Saudi Arabia

<sup>b</sup> Department of Pharmaceutics, Faculty of Pharmacy, King Abdulaziz University, Jeddah, Saudi Arabia

<sup>c</sup> Department of Clinical Pharmacology, Faculty of Medicine, King Abdulaziz University, Jeddah, Saudi Arabia

<sup>d</sup> Pharmaceutical Microbiology Department, Faculty of Pharmacy, Tanta University, Tanta 31527, Egypt

<sup>e</sup> Department of Chemistry, College of Science and Humanities in Al-Kharj, Prince Sattam bin Abdulaziz University, Al-Kharj 11942, Saudi Arabia

### ARTICLE INFO

#### Keywords:

Quinazolinone  
Breast cancer  
MDA-MB-231  
Molecular docking  
Flow cytometry  
MTT assay  
Apoptosis

### ABSTRACT

Triple-negative breast cancer (TNBC) comprises 10 % to 20 % of breast cancer, however, it is more dangerous than other types of breast cancer, because it lacks druggable targets, such as the estrogen receptors (ER) and the progesterone receptor (PR), and has under expressed receptor tyrosine kinase, ErbB2. Present targeted therapies are not very effective and other choices include invasive procedures like surgery or less invasive ones like radiotherapy and chemotherapy. This study investigated the potential anticancer activity of some novel quinazolinone derivatives that were designed on the structural framework of two approved anticancer drugs, Ispinesib (KSP inhibitor) and Idelalisib (PI3K $\delta$  inhibitor), to find out solutions for TNBC. All the designed derivatives (3a-l) were subjected to extra precision molecular docking and were synthesized and spectrally characterized. *In vitro* enzyme inhibition assay of compounds (3a, 3b, 3e, 3g and 3h) revealed their nanomolar inhibitory potential against the anticancer targets, KSP and PI3K $\delta$ . Using MTT assay, the cytotoxic potential of compounds 3a, 3b and 3e were found highest against MDA-MB-231 cells with an IC<sub>50</sub> of 14.51  $\mu$ M, 16.27  $\mu$ M, and 9.97  $\mu$ M, respectively. Remarkably, these compounds were recorded safe against the oral epithelial normal cells with an IC<sub>50</sub> values of 293.60  $\mu$ M, 261.43  $\mu$ M, and 222  $\mu$ M, respectively. The anticancer potential of these compounds against MDA-MB-231 cells was revealed to be associated with their apoptotic activity. This was established by examination with the inverted microscope that revealed the appearance of various apoptotic features like cell shrinkage, apoptotic bodies, and membrane blebbing. Using flow cytometry, the Annexin V/PI-stained cancer cells showed an increase in early and late apoptotic cells. In addition, DNA fragmentation was revealed to occur after treatment with the tested compounds by gel electrophoresis. The relative gene expression of pro-apoptotic and anti-apoptotic genes revealed an overexpression of the *P53* and *BAX* genes and a down-regulation of the *BCL-2* gene by real-time PCR. So, this work proved that compounds 3a, 3b, and 3e could be developed as anticancer candidates, via their P53-dependent apoptotic activity.

### 1. Introduction

The increased cancer incidence, as well as its high mortality rate worldwide, greatly drawn the devotion of the researchers in the past decades (Sung et al., 2021). Various therapies and interventions like chemotherapy, surgery, immunotherapy, and radiotherapy have been widely used to combat this lethal ailment (Chen et al., 2015). The most

common approach to treat cancers is chemotherapy (Debela et al., 2021). The chief concern about chemotherapy is their adverse effects that affect the quality of patient's life. The chemotherapeutic drugs have many side effects as they affect the tumour with the production of reactive oxygen species (ROS) (Anand et al., 2022). Also, normal cells are also negatively affected by many cancer therapies (Navya et al., 2019). The adverse effect includes alopecia, nausea, vomiting, fatigue,

\* Corresponding author.

E-mail address: [m.alossaimi@psau.edu.sa](mailto:m.alossaimi@psau.edu.sa) (M.A. Alossaimi).

<https://doi.org/10.1016/j.jpsps.2024.101971>

Received 17 December 2023; Accepted 30 January 2024

Available online 3 February 2024

1319-0164/© 2024 The Author(s). Published by Elsevier B.V. on behalf of King Saud University. This is an open access article under the CC BY-NC-ND license (<http://creativecommons.org/licenses/by-nc-nd/4.0/>).

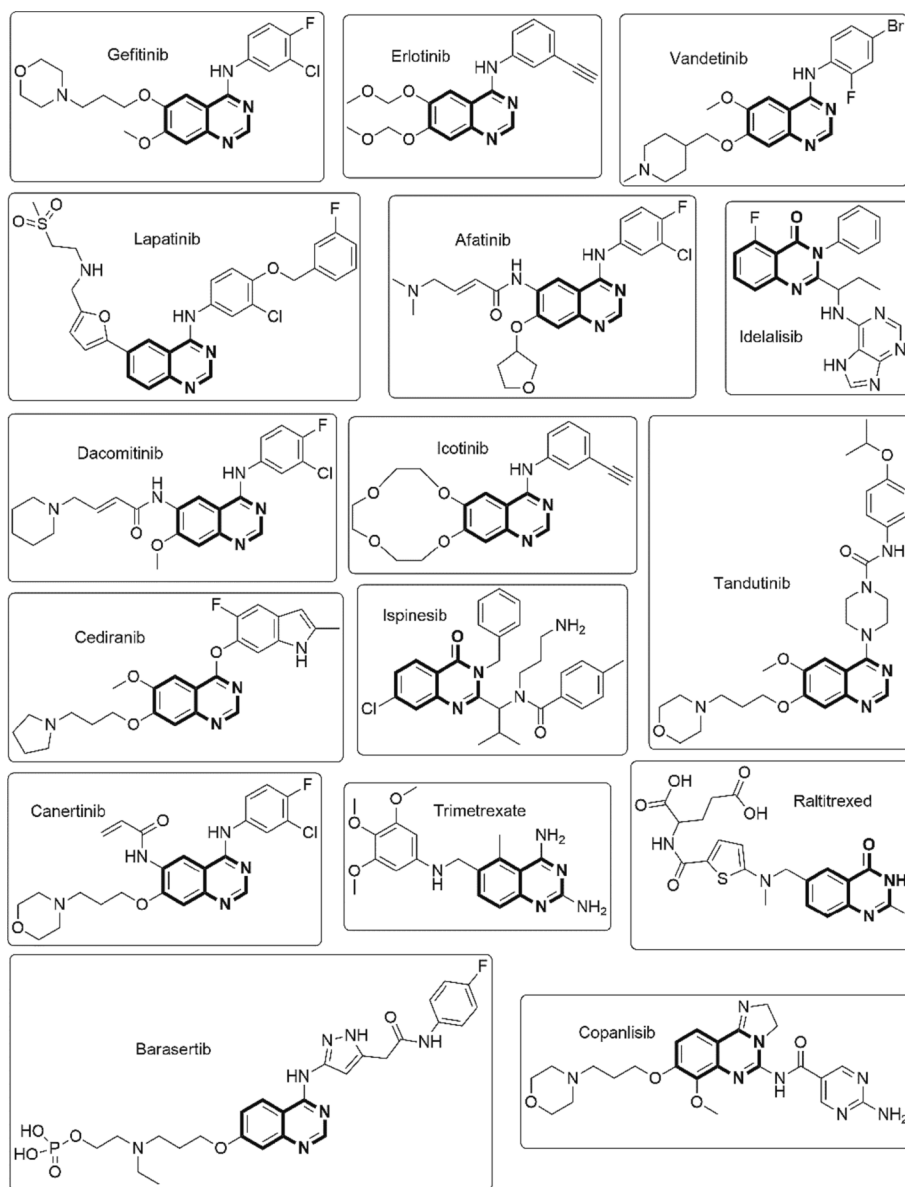


Fig. 1. FDA-approved anticancer drugs having quinazoline or quinazolinone moiety.

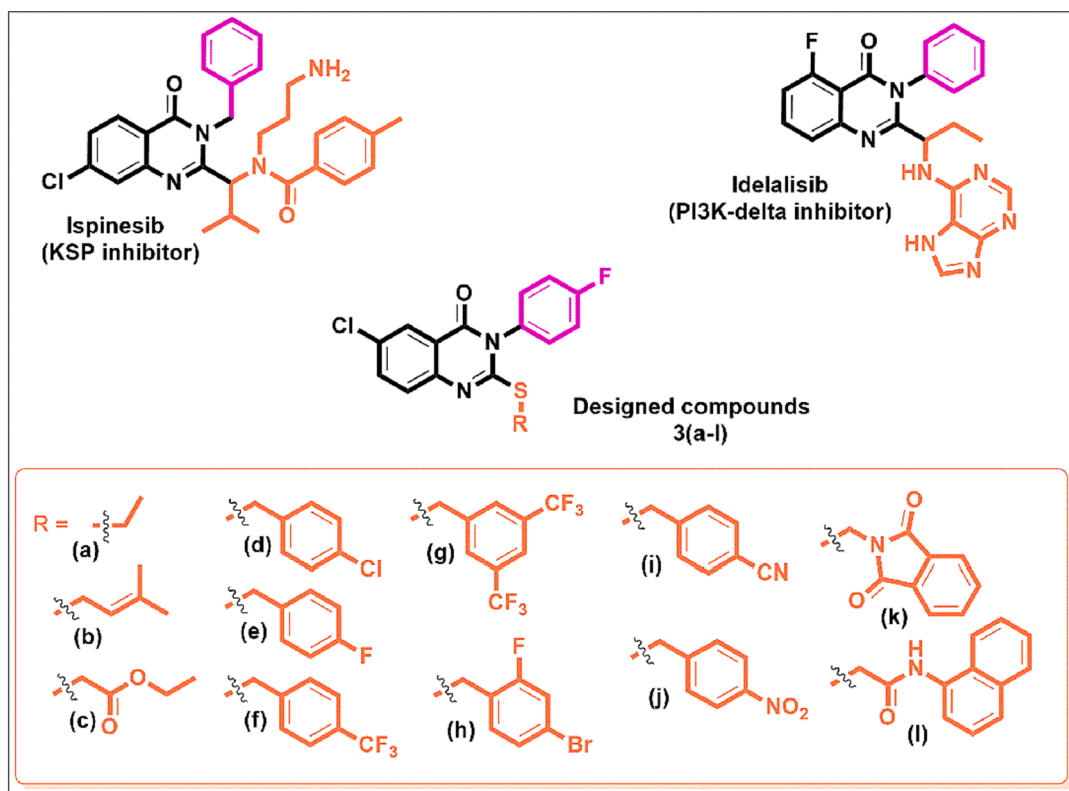


Fig. 2. Design of quinazolinone derivatives (3a-l) as anticancer agents.

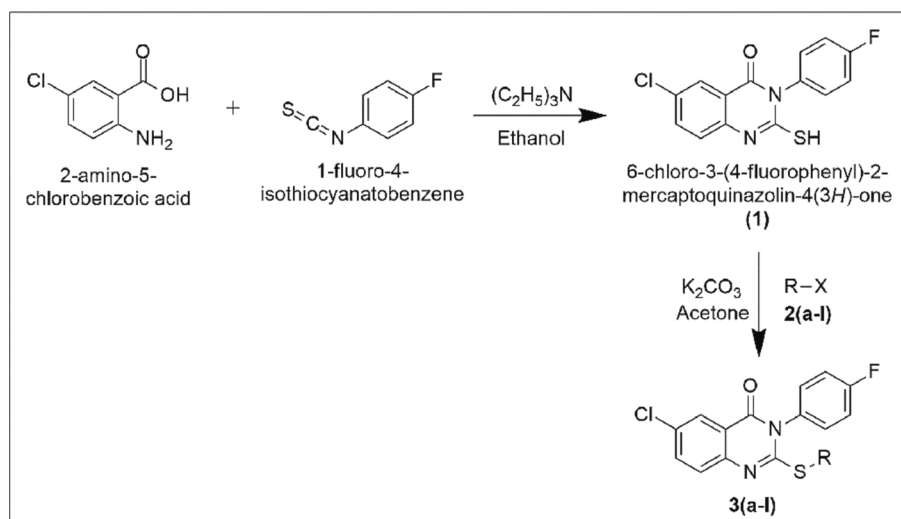


Fig. 3. Scheme for the synthesis of designed compounds (3a-l).

severe pain and even death in some instances (Aslam et al., 2014). Hence, the discovery and development of novel targeted cancer chemotherapeutics with precise efficacy and safety is an unmet medical need.

Breast cancer is a heterogeneous and most common cancer type in women. It has been recorded that there were nearly 2 million cancer cases in the past decade. Breast cancer represents about 11.6 % of the total number of cancer cases (Łukasiewicz et al., 2021). Hormone receptor + ve breast cancers characterized by upregulated ER (estrogen receptors), PR (progesterone receptors) and HER2 (epidermal growth factor receptor 2) are generally treated with endocrine therapy and agents that blocks HER2 signalling (Li et al., 2016). However, the other

type of breast cancer that does not overexpress these receptors is hard-to-treat and called as hormone receptor -ve breast cancers or triple-negative breast cancer (TNBC). TNBC comprises 10 %–20 % of breast cancer, however, it is more dangerous than other breast cancer types, because it lacks druggable targets, such as ER and PR, and has under expressed receptor tyrosine kinase, ErbB2 (often referred to HER2) (Wang et al., 2015; Liu et al., 2018; Van Swearingen et al., 2017). Consequently, new therapeutics are essential for the treatment of TNBC.

The heterocyclic moiety “Quinazoline” has emerged as a promising scaffold for anticancer drug development. Quinazoline containing drugs have been reported to inhibit various kinases overexpressed in cancer cells and were approved by various food and drug administrations (FDA)

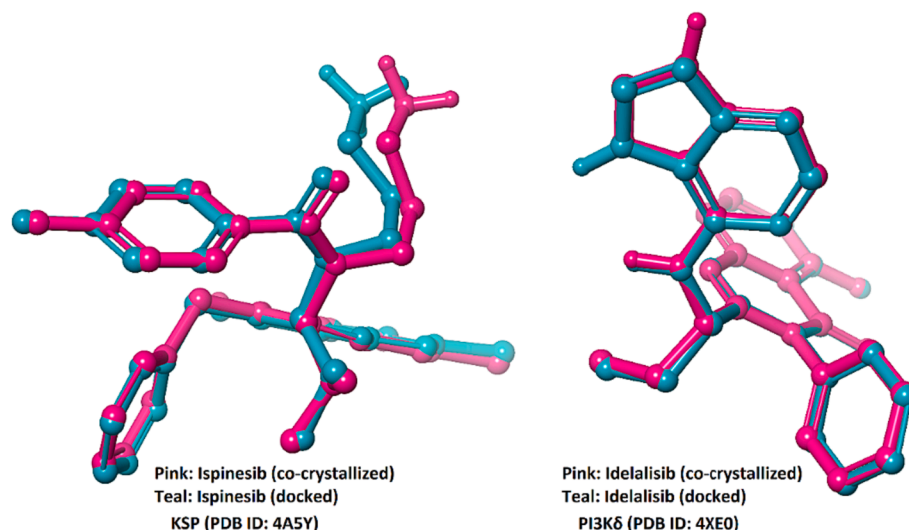


Fig. 4. Validation of the docking methodology.

**Table 1**

XP Gscore and Glide emodel of docked ligands after extra-precision (XP) docking.

Ligands	KSP (PDB ID: 4A5Y)		PI3Kδ (PDB ID: 4XE0)	
	XP Gscore (kcal/mol)	Glide emodel (kcal/mol)	XP Gscore (kcal/mol)	Glide emodel (kcal/mol)
Ispinesib	-8.62	-83.34	—	—
Idelalisib	—	—	-7.86	-66.29
1	-4.87	-46.35	-5.00	-39.78
3a	-6.61	-60.97	-6.13	-56.72
3b	-6.73	-62.42	-5.81	-55.02
3c	-5.88	-51.53	-2.38	-44.52
3d	-6.09	-56.92	-5.56	-45.07
3e	-7.05	-62.12	-5.94	-53.59
3f	-6.10	-46.12	-5.52	-47.95
3g	-6.92	-60.60	-6.61	-56.23
3h	-7.00	-64.60	-6.04	-54.71
3i	-6.42	-50.99	-5.31	-51.98
3j	-4.60	-54.03	-5.35	-38.90
3k	-5.25	-49.16	-5.27	-44.95
3l	-4.06	-50.45	-5.03	-34.13

over the years (Zayed, 2023; Ayala-Aguilera et al., 2021). Fig. 1 depicts various quinazoline/quinazolinone containing FDA-approved anticancer drugs. Ispinesib is a quinazolinone containing potent kinesin spindle protein (KSP) inhibitor. It is an allosteric inhibitor of KSP kinesin motor ATPase. The inhibition of KSP disrupts mitotic spindle formation and arrest the progression of cell cycle and ultimately cause apoptosis. It was shown to have promising results in breast cancer treatments (Purcell et al., 2010). Another, structurally similar quinazolinone containing anticancer drug is Idelalisib. It is first-in-class phosphatidylinositol 3-kinase (PI3K) inhibitor that more specifically blocks the delta isoform of PI3K, i.e PI3Kδ. It boosts antitumor response by modulating the immune response in tumor microenvironment (Lannutti et al., 2011). Based on the structural framework of these two drugs, some novel quinazolinone derivatives with varying substitution at position 2 connected through the thioether linkage, were designed to study their anticancer potential, as depicted in Fig. 2. The designed compounds (3a-l) were studied for their binding potential on the targets of Ispinesib and Idelalisib by extra

precision docking (Molecular docking). These derivatives were synthesized, characterized by various spectral techniques, and studied comprehensively for their anticancer potential.

## 2. Materials and methods

### 2.1. General: Instruments and reagents

The reaction was monitored throughout the reaction time by thin-layer chromatography (TLC) along with UV or I<sub>2</sub> vapor chamber. The melting point (MP) of prepared derivatives were recorded by Dynalco Stuart apparatus. The <sup>1</sup>H and <sup>13</sup>C NMR spectra were recorded by BRUCKER-PLUS NMR spectrometer in solvents like deuterated dimethyl sulfoxide (DMSO-d<sub>6</sub>) or deuterated chloroform (CDCl<sub>3</sub>) at 500 MHz and 125 MHz, respectively. The spectra of all the prepared derivatives are provided in the supporting materials. KBr pellet of the compounds were used to record IR spectra. All the reagents, chemicals and solvents were obtained from AK Scientific or Sigma-Aldrich. The route of synthesis is depicted in Fig. 3.

### 2.2. Extra-precision (XP) molecular docking

2D structure of the ligands (Ispinesib, Idelalisib and compounds 1 & 3a-l) were sketched on ChemDraw Ultra (v. 12) and collected in structure-data format (sdf). The protonation and tautomerization of the ligands at pH 7.2 was performed by LigPrep and Epik programs available in Maestro, Schrodinger (v. 9.4). All the structures were subjected to energy minimization for extra-precision (XP) molecular docking by Glide. The X-ray structures of crystallized Eg5 human kinesin with Ispinesib (PDB ID: 4A5Y) (Kaan et al., 2013) and PI3K delta p110 subunit with Idelalisib (PDB ID: 4XE0) (Somoza et al., 2015) were retrieved from protein data bank (PDB). Protein preparation wizard available in Maestro was used for protein structure's correction and preparation, like removal of H<sub>2</sub>O, correction of bond orders, incorporation of H atoms, and correction of charge. Hydrogen bonding network was corrected afterwards, and energy of the structures were minimized by OPLS force field to root mean square deviation (RMSD) of 0.3 Å, keeping the heavy atoms fixed. Grids around the binding sites of 20 Å size was created by

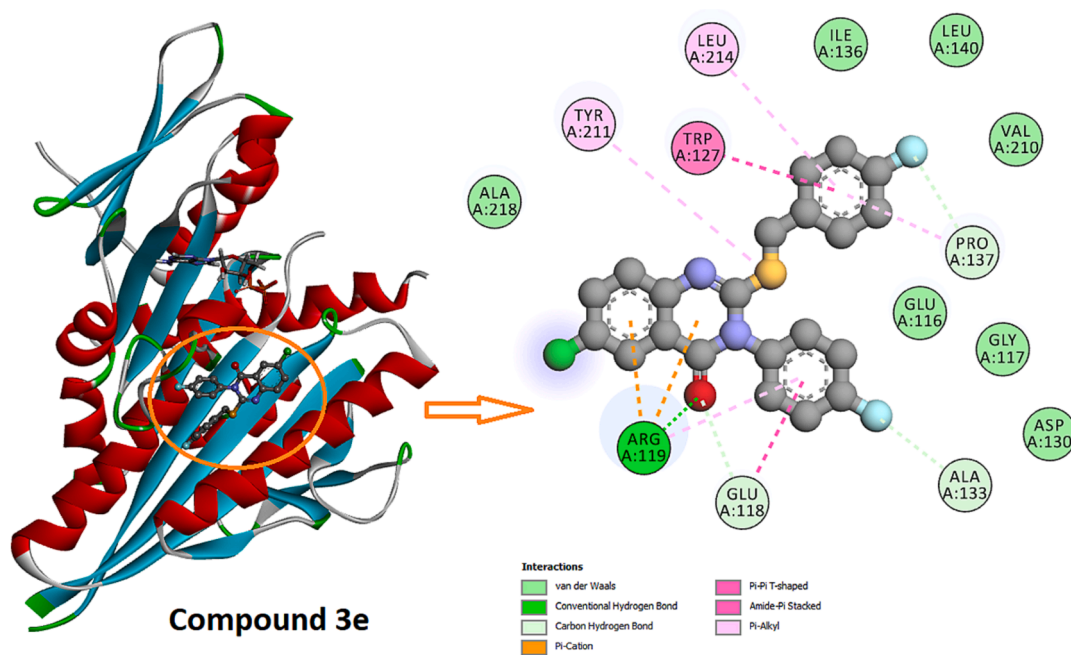


Fig. 5a. Interaction pose of compound 3e with KSP.

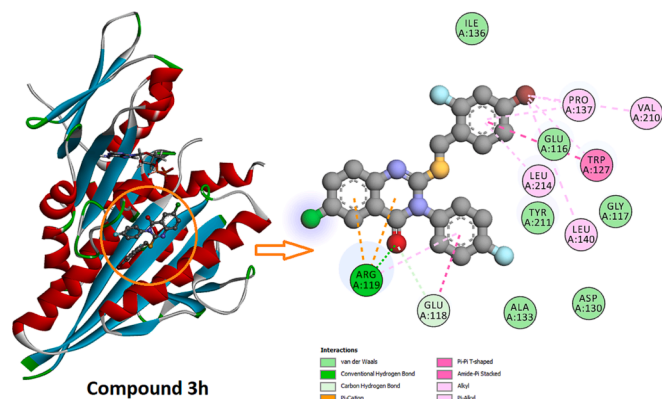


Fig. 5b. Interaction pose of compound 3h with KSP.

the program glide grid. Glide, Maestro was used for XP docking of the prepared ligands (Friesner et al., 2006). The two- and three-dimensional interactions of the ligands within the active site of protein structures were recorded by Discovery Studio software.

## 2.3. In vitro inhibition assay

### 2.3.1. Inhibition of KSP ATPase activity

The *in vitro* KSP ATPase inhibition assay of the selected five compounds (3a, 3b, 3e, 3g and 3h) having good glide XP score, was performed by the microtubule-activated ATPase end-point assay kit (Cytoskeleton, Cat. # BK053) at 2  $\mu$ M concentrations in triplicate, as per the manufacturer's instructions (Funk et al., 2004). The selected compounds and Ispinesib (positive control) were dissolved in DMSO. In short, KSP (0.4  $\mu$ g), test compounds (2  $\mu$ M) and microtubules (2  $\mu$ g) were taken in 96-well half-area plates. ATP (0.3 mM) was added, and the wells were incubated at room temperature for five minutes. The reaction

was then terminated by adding CytoPhos reagent (70  $\mu$ l). The wells were then further incubated for additional ten minutes and absorbance was measured at 650 nm by a spectrophotometer. For IC<sub>50</sub> value measurement, a microtubule-activated ATPase kinetic assay kit (Cytoskeleton, Cat. # BK060) was used as per the manufacturer's instructions (Webb, 1992). The assay was performed for eight different concentrations of test compounds (3a, 3b, 3e, 3g, 3h and Ispinesib) in triplicate.

### 2.3.2. Inhibition of PI3K $\delta$ activity

The *in vitro* PI3K $\delta$  inhibition assay of the selected compounds was performed by the assay kit (BPS Bioscience, Cat. # 79799) at eight different concentrations of test compounds (3a, 3b, 3e, 3g, 3h and Idelalisib) in triplicate, as per the manufacturer's instructions (Zhao et al., 2017). In brief, to each well, 5  $\mu$ l PI3K lipid substrate, 5  $\mu$ l test sample (inhibitor well) or inhibitor buffer (blank well), 5  $\mu$ l ATP (12.5  $\mu$ M), and 10  $\mu$ l of kinase buffer (2x) to blank wells only, was added. 10  $\mu$ l of diluted PI3K $\delta$  enzyme was added to the test wells to initiate the reaction and incubated for 40 min at room temperature. 25  $\mu$ l of ADP-Glo reagent was added to each well and further incubated for 45 min. 50  $\mu$ l of kinase detection reagent was added and further incubated for 30 min under light protection. Luminescence intensity was measured using a microplate reader, and IC<sub>50</sub> values were calculated using GraphPad prism.

## 2.4. In vitro anticancer activity

### 2.4.1. Cell lines and chemicals

The oral epithelial normal cells and MDA-MB-231 cells were preserved in Dulbecco's Modified Eagle's Medium (DMEM) with 10 % (v/v) fetal bovine serum (FBS) and 1 % (v/v) streptomycin/penicillin. The cells in the standard medium were incubated in 5 % CO<sub>2</sub> incubator (NUAIRE, USA) at 37 °C before performing the experiment. Doxorubicin was purchased from Pharmacia (Egypt) and all other utilized chemicals were purchased from Merck (UK).

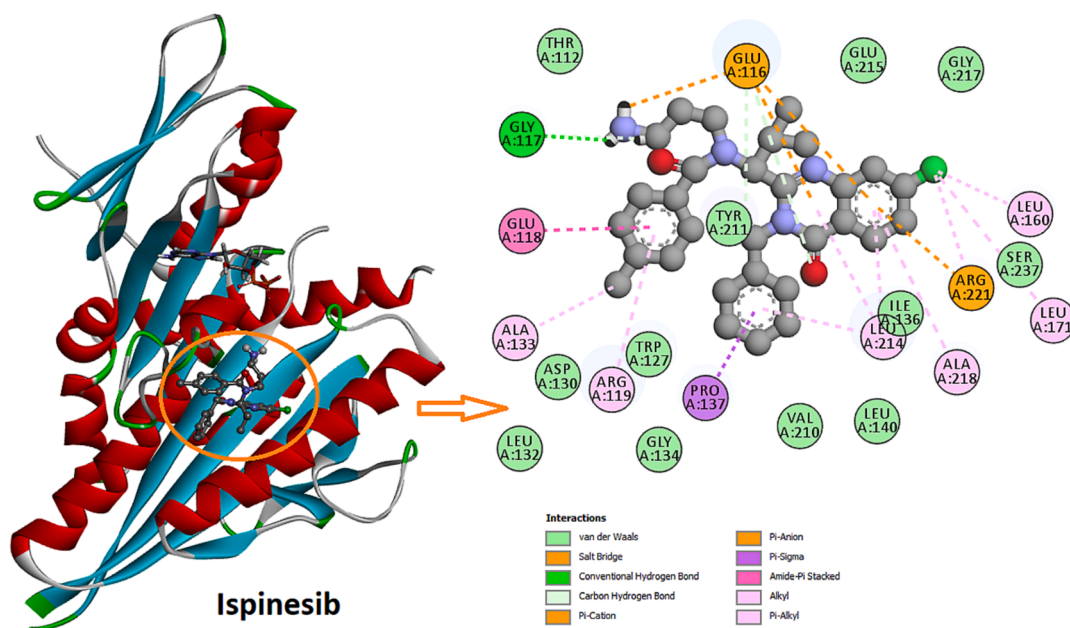


Fig. 5c. Interaction pose of Ispinesib with KSP.

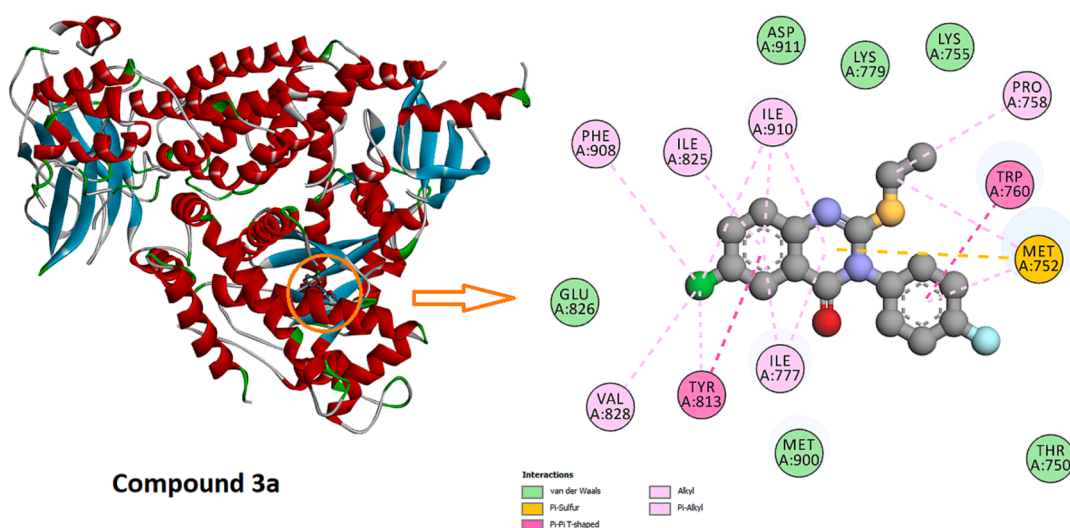


Fig. 6a. Interaction pose of compound 3a with PI3K6.

#### 2.4.2. MTT assay

MDA-MB-231 cells as well as the oral epithelial normal cells were seeded into 96-well cell culture plates. The concentration of about  $10^4$  cells/ml was incubated for 24 h at typical conditions to attain sufficient growth. Cells were subjected to separate concentrations of the tested compounds (6.25, 12.5, 25, 50, and 100  $\mu\text{g/ml}$ ) dissolved in dimethyl sulfoxide (DMSO). The cells and drug mixtures were incubated for 24 and 48 h. After the specified time, the utilized medium was discarded, and each well was supplied with 5 mg/mL of MTT reagent, then they were left for three to four hours (Alotaibi et al., 2021; Attallah et al., 2022). The viable cells that formed formazan crystals were detected by dissolving in 100  $\mu\text{l}$  acidified isopropanol. The results were recorded at 630 nm by an ELISA reader (Malongane et al., 2022; Alotaibi et al., 2021). Cell viability was determined as follows:

$$\text{Cell viability percentage} = \frac{\text{Absorbance of the drug treated cells}}{\text{Absorbance of the cells without drugs}} \times 100$$

#### 2.4.3. Morphological studies

The changes that occurred phenotypically in MDA-MB-231 cells, after treatment with varying concentration of tested compounds post 48 h, were elucidated by an inverted microscope (Leica, Germany) (Rahman et al., 2016).

#### 2.4.4. Flow cytometry studies

The induction of apoptosis as well as necrosis after 48 h of treatment of MDA-MB-231 cells with the tested compounds was investigated by Novocyte Flow Cytometer (Acea Biosciences, USA). After harvesting the MDA-MB-231 cells, they were rinsed and suspended in 100  $\mu\text{l}$  phosphate-buffered saline (PBS). Tested cells were then stained with 10  $\mu\text{l}$  Annexin V-FITC/propidium iodide solution. The flow cytometry analysis was performed after incubating the mixture for 20 min in a dark room (Noh et al., 2021; Murad et al., 2016).

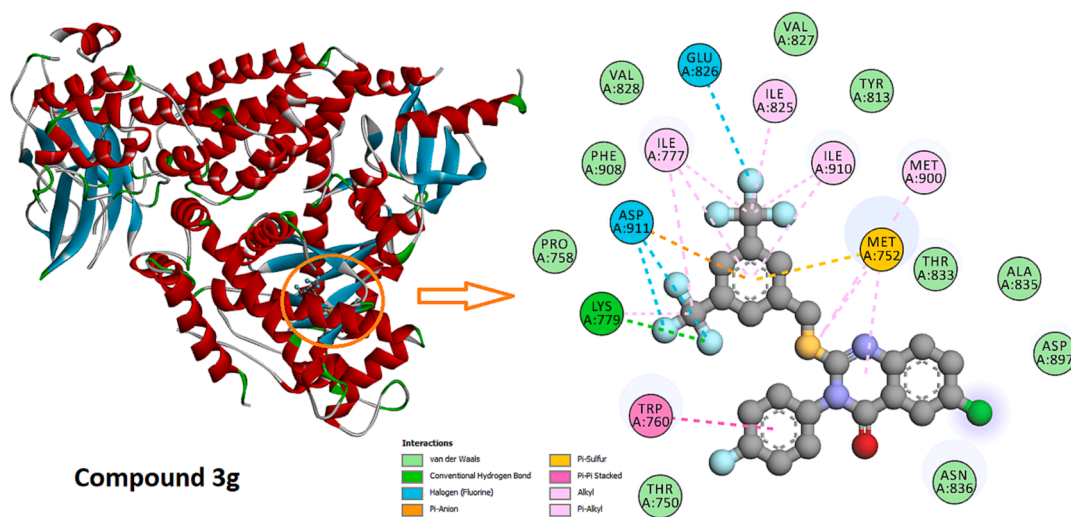


Fig. 6b. Interaction pose of compound 3 g with PI3Kδ.

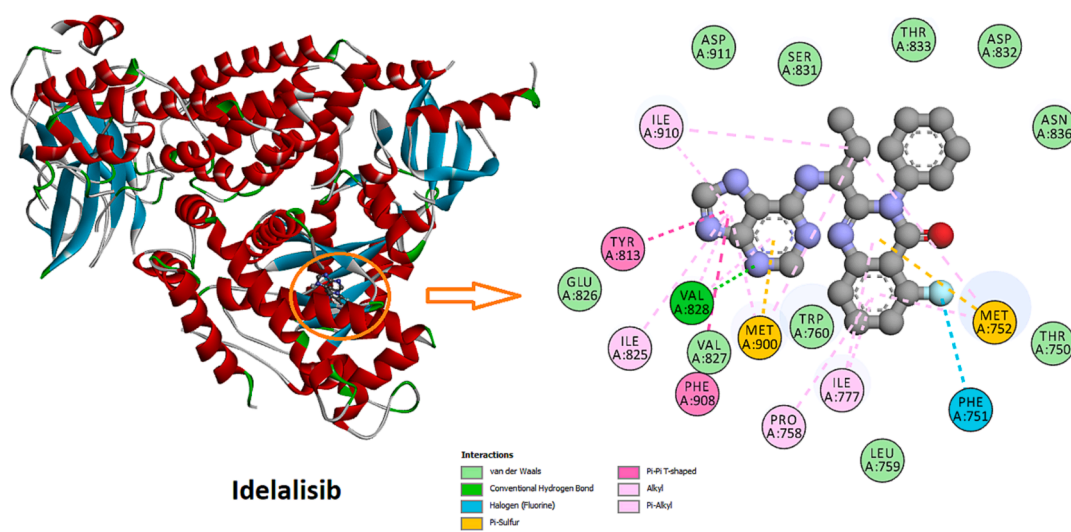


Fig. 6c. Interaction pose of Idelalisib with PI3Kδ.

Table 2

Inhibition assay of the synthesized quinazolinone compounds (3a, 3b, 3e, 3 g, and 3 h) against KSP (% inhibition at 2  $\mu$ M and IC<sub>50</sub>), using Ispinesib as positive control, and against PI3K $\delta$  using Idelalisib as positive control.

Compound	KSP ATPase inhibition [%] <sup>a</sup> (IC <sub>50</sub> [nM]) <sup>b</sup>	PI3K $\delta$ activity (IC <sub>50</sub> [nM]) <sup>b</sup>
3a	88.35 $\pm$ 3.86 % (88.65 $\pm$ 3.15)	38.21 $\pm$ 2.15
3b	89.62 $\pm$ 3.42 % (85.80 $\pm$ 3.35)	32.28 $\pm$ 2.18
3e	93.28 $\pm$ 2.10 % (68.42 $\pm$ 2.65)	45.35 $\pm$ 2.05
3g	90.55 $\pm$ 2.16 % (77.42 $\pm$ 3.32)	57.75 $\pm$ 2.75
3h	92.62 $\pm$ 2.35 % (73.45 $\pm$ 2.86)	53.82 $\pm$ 3.10
Ispinesib	95.48 $\pm$ 2.24 % (1.42 $\pm$ 0.13)	—
Idelalisib	—	3.55 $\pm$ 0.18

<sup>a</sup> % Inhibition values are KSP ATPase inhibition at 2  $\mu$ M and are shown as mean  $\pm$  SD (n = 3).

<sup>b</sup> IC<sub>50</sub> values are shown as mean  $\pm$  SD (n = 3), using eight different concentrations of test compounds and positive controls.

#### 2.4.5. DNA fragmentation

DNA was extracted from the MDA-MB-231 cells pre- and post-treatment with the tested compounds using a DNA extraction kit (Qiagen, USA) following the manufacturer's instructions. The extracted DNA

was tested for quality using a nanodrop spectrophotometer (Thermo Scientific, USA). Then, 1X loading dye was supplemented to the extracted DNA, and the mixture was run on the agarose gel. DNA fragmentation was visualized using a UV transilluminator, and photos were taken using Gel Doc (Bio-rad, USA) (Samarghandian et al., 2013).

#### 2.4.6. qRT-PCR

RNA was extracted from the cells after 48 h of treatment, using MiniKit (PureLink™, Invitrogen, USA) and its purity was established by a nanodrop spectrophotometer (Thermo Scientific, USA). The genes *P53*, *BAX*, and *BCL-2*, were studied using *B-actin* as a housekeeping gene. The cDNA was manufactured using SuperScript™ III First-Strand Synthesis kit (Thermo Fischer, USA). The RT-PCR was conducted using Rotor-Gene Q (Qiagen, USA). The utilized primers sequences are shown in Table S1 (Ramadan et al., 2019).

#### 2.5. Statistics

All the performed tests were repeated thrice and revealed as mean  $\pm$  SD. ANOVA test was employed to elucidate the variance between the treated and untreated cells. GraphPad Prism (ver. 8) was used for the statistical analysis. Differences between the tested groups were regarded

**Table 3**  
*In vitro* Anticancer activity of the compounds by MTT assay.

Compound	MDA-MB-231 breast cancer cells		Oral epithelial normal cells
	IC <sub>50</sub> after 24 h in $\mu\text{g/mL}$ ( $\mu\text{M}$ )	IC <sub>50</sub> after 48 h in $\mu\text{g/mL}$ ( $\mu\text{M}$ )	IC <sub>50</sub> after 48 h in $\mu\text{g/mL}$ ( $\mu\text{M}$ )
1	13.60 $\pm$ 0.12 (44.34 $\pm$ 0.39)	7.23 $\pm$ 0.15 (23.57 $\pm$ 0.48)	80.03 $\pm$ 1.05 (260.90 $\pm$ 3.42)
3a	9.54 $\pm$ 0.11 (28.49 $\pm$ 0.32)	4.86 $\pm$ 0.18 (14.51 $\pm$ 0.53)	98.30 $\pm$ 1.20 (293.60 $\pm$ 3.58)
3b	17.80 $\pm$ 0.12 (47.48 $\pm$ 0.32)	6.10 $\pm$ 0.10 (16.27 $\pm$ 0.26)	98.00 $\pm$ 1.31 (261.43 $\pm$ 3.49)
3c	22.00 $\pm$ 0.13 (56.00 $\pm$ 0.33)	7.01 $\pm$ 0.12 (17.84 $\pm$ 0.30)	58.28 $\pm$ 1.15 (148.36 $\pm$ 2.92)
3d	9.05 $\pm$ 0.10 (20.98 $\pm$ 0.23)	6.59 $\pm$ 0.09 (15.27 $\pm$ 0.20)	65.40 $\pm$ 1.30 (151.63 $\pm$ 3.01)
3e	8.94 $\pm$ 0.08 (21.54 $\pm$ 0.19)	4.14 $\pm$ 0.11 (9.97 $\pm$ 0.26)	92.10 $\pm$ 1.40 (222.00 $\pm$ 3.37)
3f	27.39 $\pm$ 0.10 (58.92 $\pm$ 0.21)	17.19 $\pm$ 0.12 (36.97 $\pm$ 0.25)	67.80 $\pm$ 1.20 (145.85 $\pm$ 2.58)
3g	26.92 $\pm$ 0.09 (50.51 $\pm$ 0.17)	20.32 $\pm$ 0.23 (38.13 $\pm$ 0.43)	70.40 $\pm$ 1.90 (132.11 $\pm$ 3.56)
3h	14.89 $\pm$ 0.11 (30.15 $\pm$ 0.22)	8.14 $\pm$ 0.13 (16.48 $\pm$ 0.26)	51.40 $\pm$ 1.50 (104.10 $\pm$ 3.03)
3i	40.33 $\pm$ 0.11 (95.59 $\pm$ 0.26)	26.49 $\pm$ 0.13 (62.79 $\pm$ 0.30)	86.45 $\pm$ 1.50 (204.92 $\pm$ 3.55)
3j	22.48 $\pm$ 0.12 (50.87 $\pm$ 0.27)	13.96 $\pm$ 0.12 (31.59 $\pm$ 0.27)	78.30 $\pm$ 1.40 (177.20 $\pm$ 3.16)
3k	17.71 $\pm$ 0.14 (38.01 $\pm$ 0.30)	8.57 $\pm$ 0.10 (18.39 $\pm$ 0.21)	80.50 $\pm$ 1.20 (172.79 $\pm$ 2.57)
3l	13.18 $\pm$ 0.13 (26.90 $\pm$ 0.26)	6.98 $\pm$ 0.12 (14.24 $\pm$ 0.24)	79.00 $\pm$ 1.30 (161.24 $\pm$ 2.65)
Doxorubicin	—	0.77 $\pm$ 0.14 (1.41 $\pm$ 0.25)	40.5 $\pm$ 0.86 (74.51 $\pm$ 1.57)

to be significant if  $p$ -value  $<$  0.05.

### 3. Results

#### 3.1. Synthesis and spectral characterization

The procedure followed for the synthesis of the derivatives (3a-l) started with the dropwise addition of 4-Fluorophenyl isothiocyanate (1 mmol) with stirring into the solution of 5-chloroanthranilic acid (1 mmol) in ethanol (20 ml) containing catalytic amount of triethylamine (1.1 mmol). The reaction mixture was refluxed for about two hours. The obtained solid was recrystallized with ethanol that afforded pure intermediate compound 1. This intermediate compound 1 (1 mmol) was refluxed with different alkyl or aryl halides (1 mmol) in the presence of anhydrous potassium carbonate (1.5 mmol) in solvent acetone (10 ml) for about ten hours. The progress of the reactions was continuously monitored by TLC. After reaction completion, the mixture was cooled and obtained solid was filtered and dried. The crude product was recrystallized from EtOH to attain the final products (3a-l). The spectra and data proving successful synthesis of the derivatives is provided in the [supporting material](#).

#### 3.2. Extra-precision (XP) molecular docking

The molecular docking method adapted was authenticated by docking Ispinesib with human kinesin Eg5 (PDB ID: 4A5Y) (Kaan et al., 2013) and Idelalisib with p110 subunit of PI3K delta (PDB ID: 4XE0) (Somoza et al., 2015) by XP docking program of Glide. The heavy atoms of the docked poses were aligned with the pose of co-crystallized structures and found to be within 1 Å. Heavy atoms RMSD for the co-crystallized and docked poses of Ispinesib and Idelalisib were found to be 0.87 Å and 0.45 Å, respectively (Fig. 4). The docking score (glide XP score) and binding energy (glide emodel) of all the docked ligands and

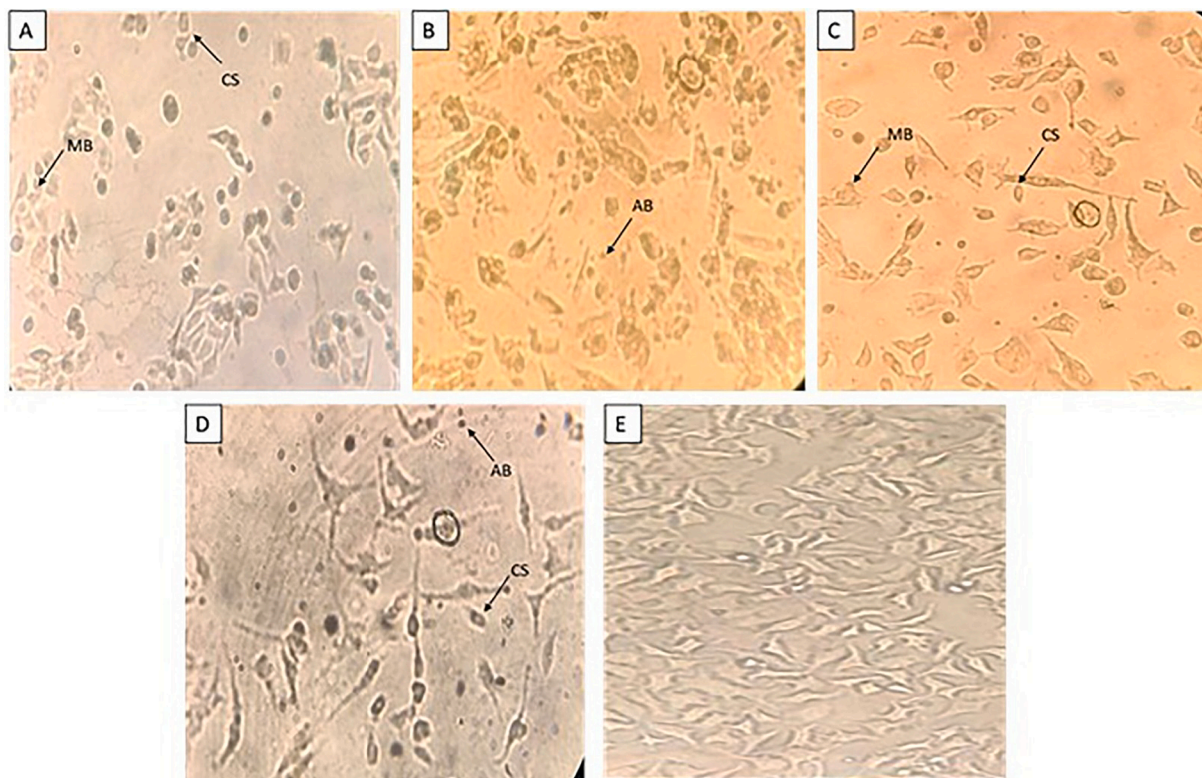


**Fig. 7.** Morphological alterations that occurred in MDA-MB-231 cells after treatment with compounds 3a (A), 3b (B), 3e (C), doxorubicin (D), and untreated cells (E). The symbol CS means cell shrinkage, Ab means apoptotic bodies, and MB membrane blebbing.

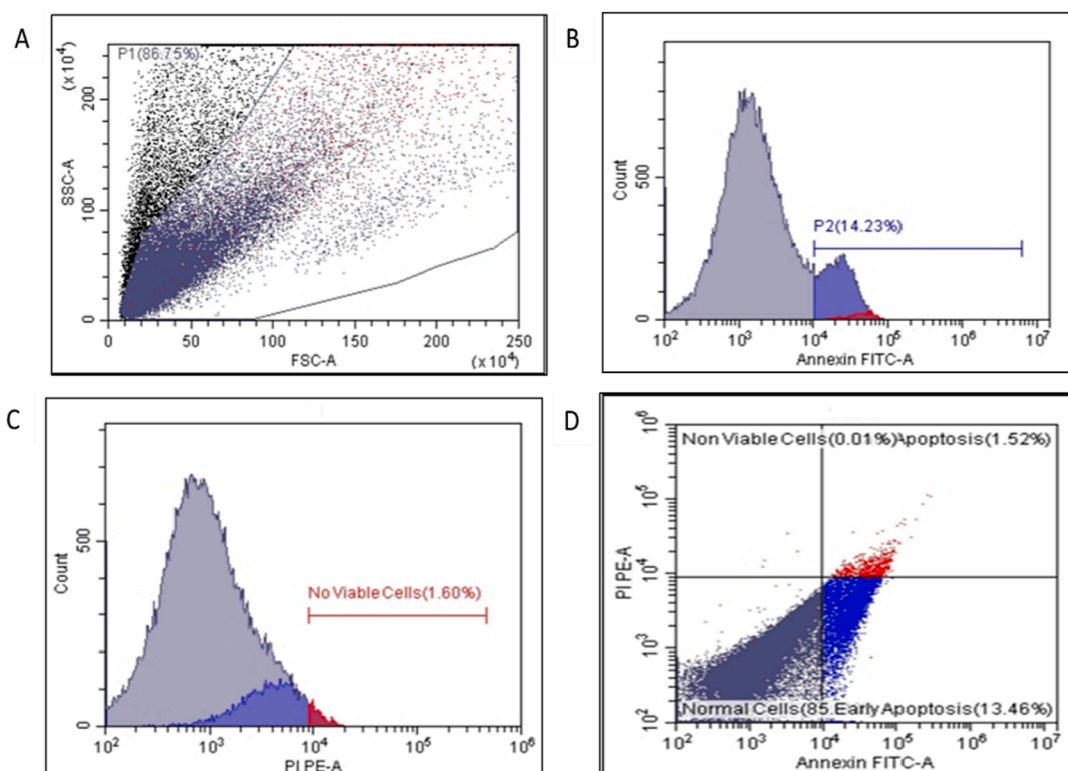


**Fig. 8.** (A and C) Flow cytometric dot plot, and (B and D) histograms for compound 3a. The staining was performed using annexin V FITC/PI dual staining method.

reference structures (Ispinesib and Idelalisib) are tabulated in [Table 1](#). Among all the thirteen docked ligands, five compounds (3a, 3b, 3e, 3g, and 3h) scored comparable scores and binding energies with the respective reference structures. The XP Gscore of compounds 3a, 3b, 3e,

3g, 3h and Ispinesib after docking with human kinesin Eg5 of KSP protein were found to be  $-6.61$ ,  $-6.73$ ,  $-7.05$ ,  $-6.92$ ,  $-7.00$ , and  $-8.62$  kcal/mol, respectively. While XP Gscore of compounds 3a, 3b, 3e, 3g, 3h and Ispinesib after docking with p110 subunit of PI3K delta

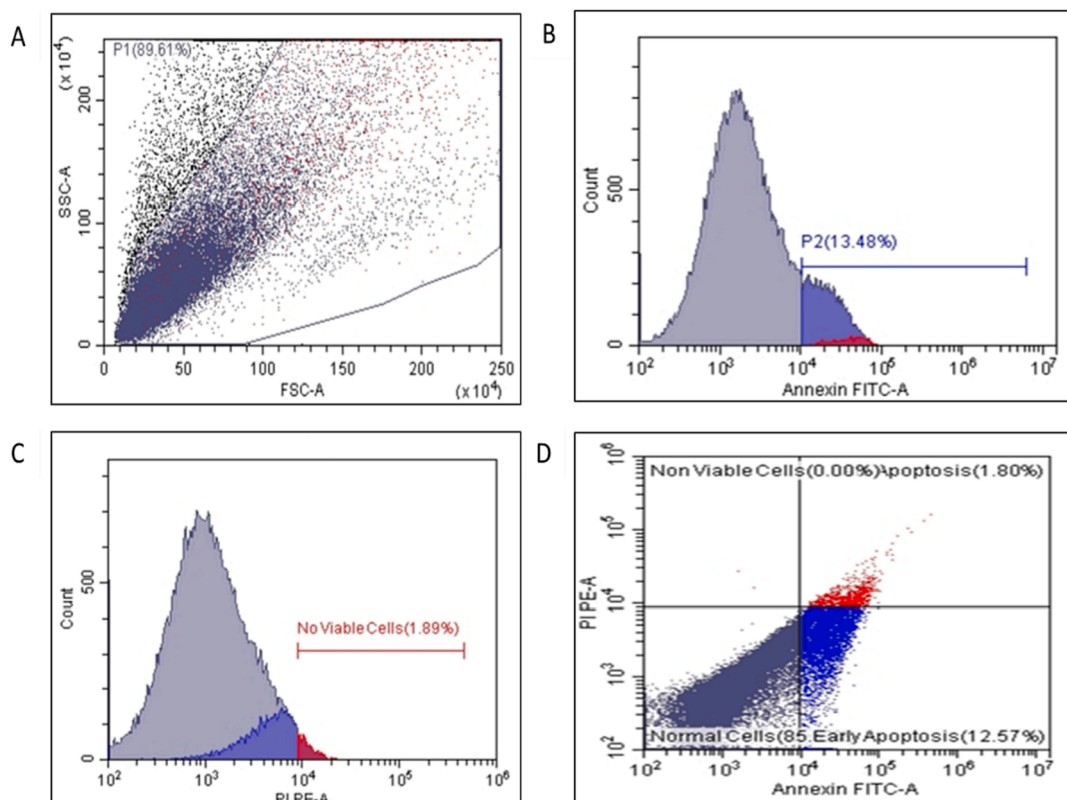


**Fig. 9.** (A and C) Flow cytometric dot plot, and (B and D) histograms for compound 3b. The staining was performed using annexin V FITC/PI dual staining method.

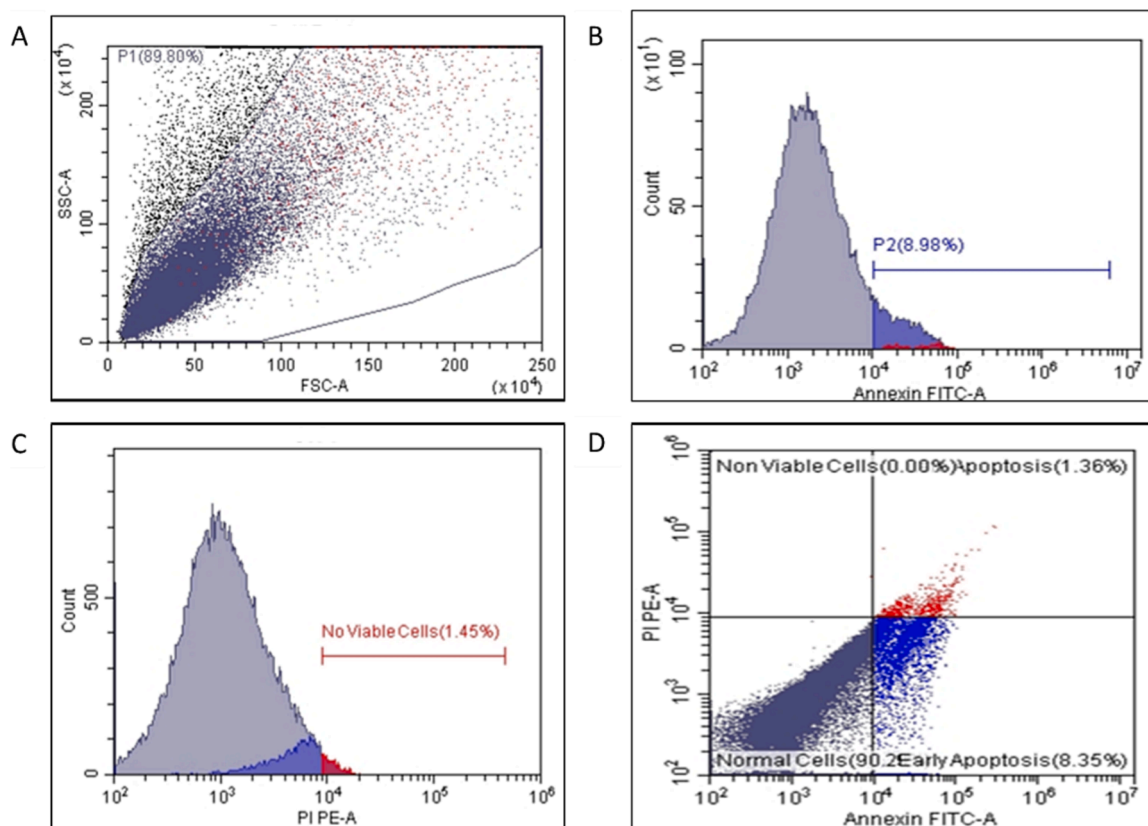


Fig. 10. (A and C) Flow cytometric dot plot, and (B and D) histograms for compound 3e. The staining was performed using annexin V FITC/PI dual staining method.

protein were found to be  $-6.13$ ,  $-5.81$ ,  $-5.94$ ,  $-6.61$ ,  $-6.04$ , and  $-7.86$  kcal/mol, respectively. Also, the binding energy (glide emodel) of these top five scoring compounds were comparable to the reference ligands. The 2D and 3D binding poses of top two scoring compounds (3e & 3 h) against KSP and compounds (3a & 3 g) against PI3K $\delta$  and reference ligands are depicted in Figs. 5a–5c and Figs. 6a–6c, respectively. The interactions of other good scoring compounds are provided in the supporting information (Figs. S1–S6).

### 3.3. *In vitro* inhibition assay (KSP ATPase and PI3K $\delta$ activity)

Five compounds having good docking scores (3a, 3b, 3e, 3 g and 3 h) were subjected to *in vitro* enzyme inhibition assay against the anticancer targets, viz. KSP and PI3K $\delta$ . At 2  $\mu$ M concentration, all the selected compounds inhibited the KSP ATPase activity up to or more than 90 %, as compared to the potent inhibitor, Ispinesib. Further assay was performed to determine their IC<sub>50</sub> values at eight different concentrations ranging from 100 nM to 0.78 nM (Table 2). All the compounds showed nanomolar potency, IC<sub>50</sub> value ranging from 68.42 to 88.65 nM, as compared to Ispinesib (1.42 nM). Compound 3e (4-fluoro) showed highest potency, followed by 3 h (2-fluoro,4-bromo), 3 g (3,5-ditri-fluoromethyl), 3b and 3a. However, in PI3K $\delta$  assay, a different pattern of inhibition was observed. Less bulky substituted derivatives, 3a (38.21 nM) and 3b (32.28 nM) showed highest potency followed by halogen substituted derivatives, viz. 3e (45.35 nM), 3 h (53.82 nM) and 3 g (57.75 nM), as compared to standard control, Idelalisib (3.55 nM).

### 3.4. *In vitro* anticancer activity

#### 3.4.1. Cytotoxic effects of the tested compounds on the oral epithelial normal cells and MDA-MB-231 cells

The IC<sub>50</sub> values of the compounds were determined by *in vitro* MTT

assay for both the oral epithelial normal cells and MDA-MB-231 cells. As shown in Table 3 and Figs. S7 and S8, compounds 3a, 3b, and 3e were found to have significantly low IC<sub>50</sub> for MDA-MB-231 cells with values of 14.51  $\mu$ M, 16.27  $\mu$ M and 9.97  $\mu$ M, respectively. In contrast, they were relatively safe on the oral epithelial normal cells with IC<sub>50</sub> values of 293.6  $\mu$ M, 261.43  $\mu$ M, and 222  $\mu$ M, respectively. So, the cytotoxic effect of these three compounds was further studied at the molecular level. The IC<sub>50</sub> of doxorubicin was 1.41  $\mu$ M for MDA-MB-231 cells and 74.51  $\mu$ M for oral epithelial normal cells after 48 h.

#### 3.4.2. Impact on cell morphology

The morphological changes that occurred in the treated cells in contrast with untreated cells are revealed in Fig. 7. After treatment with the tested compounds (3a, 3b, and 3e), observed morphological changes were cell shrinkage, apoptotic bodies formation, and membrane blebbing).

#### 3.4.3. Flow cytometry

The MDA-MB-231 cells were stained by Annexin V-FITC & PI and then studied by flow cytometry, as revealed in Figs. 8, 9, 10, 11, and 12. There was a significant increase in the number of cells in the early and late apoptosis, post-treatment with compounds 3a, 3b, and 3e in relationship with the untreated cells (Fig. 13).

#### 3.4.4. Impact on the DNA fragmentation

The influence of the synthesized derivatives (3a, 3b & 3e) on the fragmentation of the extracted DNA from the MDA-MB-231 cells was studied by gel electrophoresis. As shown in Fig. 14, internucleosomal fragmentation was noticed in the MDA-MB-231 cells, post-treatment with the tested compounds.

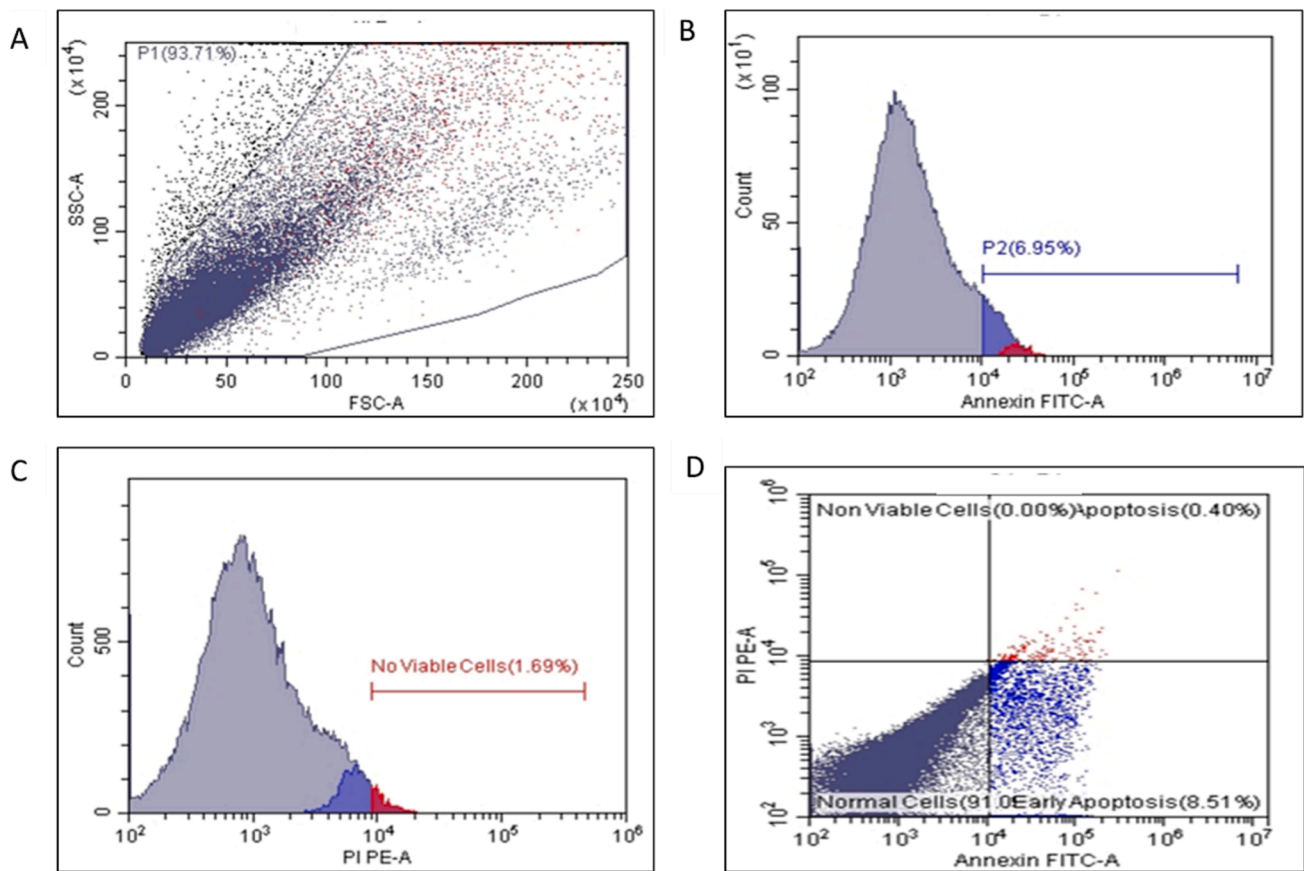


**Fig. 11.** (A and C) Flow cytometric dot plot, and (B and D) histograms for doxorubicin (standard drug). The staining was performed using annexin V FITC/PI dual staining method.

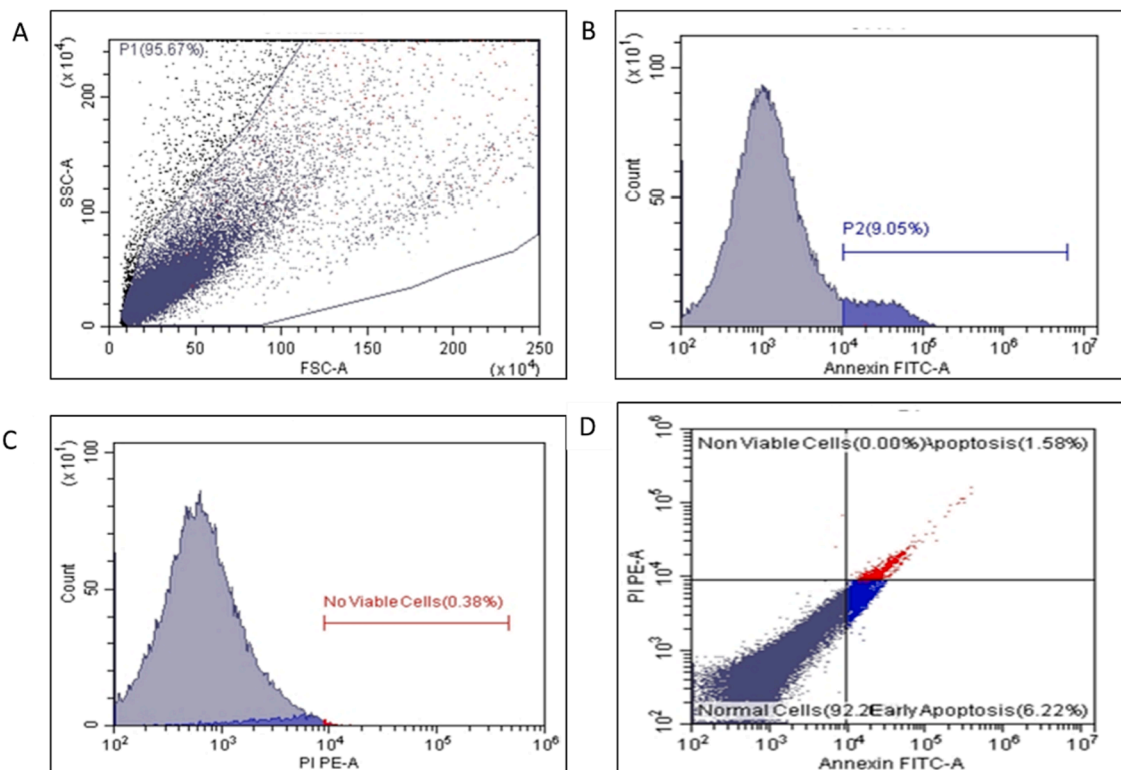


**Fig. 12.** Flow cytometric dot plot (A and C) as well as histograms (B and D) of the untreated cells. The staining was performed using annexin V FITC/PI dual staining method.

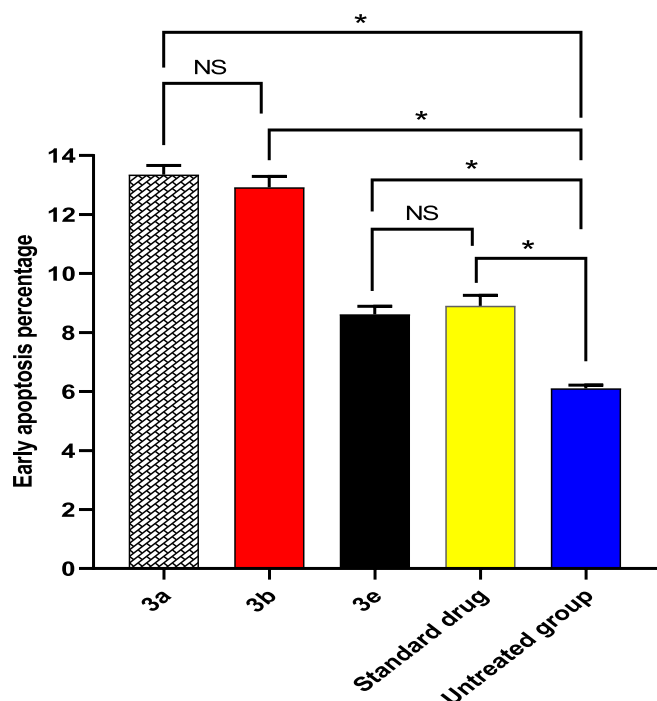


Fig. 13. Bar chart showing the early apoptosis percentage as revealed from the results of the flow cytometry. NS and \* indicates a non-significant and significant difference, respectively.

#### 3.4.5. Impact on the gene expression

The influence of compounds 3a, 3b, and 3e was revealed on the relative gene expression of *P53*, *BAX*, and *BCL-2* genes using qRT-PCR, as depicted in Fig. 15. It was observed that the tested compounds resulted in a significant overexpression of *P53* and *BAX* genes, whereas a downregulation of *BCL-2* gene was noticed.

## 4. Discussion

This study demonstrates the designing of some novel quinazoline derivatives (3a-l) based on the structural framework of two established anticancer drugs Ispinesib and Idelalisib. The designed compounds (3a-l) were synthesized efficiently by S-alkylation or arylation of 6-chloro-3-(4-fluorophenyl)-2-mercaptoquinazolin-4(3H)-one (compound 1) and their successful synthesis was validated by spectroscopic techniques. All the compounds were studied for their binding potential on two potential anticancer targets, KSP and PI3K delta. Among them, five compounds (3a, 3b, 3e, 3g, and 3h) showed promising results that were comparable to the reference structures, Ispinesib and Idelalisib. To confirm the *in-silico* results, compounds (3a, 3b, 3e, 3g and 3h) were subjected to *in vitro* inhibition assays (KSP ATPase and PI3K $\delta$  activity). At 2  $\mu$ M concentration, the compounds inhibited the KSP ATPase activity up to or more than 90%. The compounds showed nanomolar potency, IC<sub>50</sub> value ranging from 68.42 to 88.65 nM, as compared to Ispinesib (1.42 nM). In PI3K $\delta$  inhibition assay, less bulky substituted derivatives, 3a and 3b showed highest potency followed by halogen substituted derivatives, viz. 3e, 3h and 3g (IC<sub>50</sub> value ranging from 38.21 to 57.75 nM), as compared to standard control, Idelalisib (3.55 nM). However, all the compounds (3a-l & 1) were selected for further *in vitro* anticancer potential to find out the most promising molecules.

The *in vitro* anticancer study revealed the capability of the compounds to hinder the proliferation of MDA-MB-231 cells by MTT assay.

Apoptosis is an essential phenomenon for the elimination of terminally damaged cells (Su, 2020; Kumari et al., 2021; Hanahan, 2022). During this process, a series of changes occur in the cells, like shrinkage, blebbing, nuclear fragmentation, chromatin condensation, and fragmentation of the chromosomal DNA. These events finally end with cell death (Poon et al., 2014). The cytotoxic study of the compounds (3a, 3b, and 3e) on the morphology of MDA-MB-231 cells showed cell shrinkage, apoptotic bodies formation, and membrane blebbing. All such findings are features of apoptosis (Elmore, 2007; Alotaibi et al., 2021). Cells display diverse alterations throughout the early and late stages of apoptosis, like the loss of phospholipid asymmetry (Julian et al., 2015). This leads to the exposure of phosphatidylserine on the outer surface of the cell membrane. Annexin V is usually employed for the identification of apoptotic cells using flow cytometry, as it binds to phosphatidylserine. Staining the cells with Annexin V and PI can differentiate between the early (Annexin V stained and PI not stained) and late (Annexin V stained and PI stained) apoptotic cells (Lee et al., 2013). The obtained flow cytometric data of the current study designated that compound 3a, 3b, and 3e have induced the early and late stages of apoptosis in MDA-MB-231 breast cancer cells.

Nuclear DNA fragmentation is considered a biochemical hallmark of the apoptotic process (Samarghandian et al., 2013). Interestingly, this was observed in the MDA-MB-231 cells after exposure to compounds 3a, 3b, and 3e by gel electrophoresis. Also, measuring the relative expression levels of the genes that regulate apoptosis (*P53*, *BAX*, and *BCL-2*) was performed in this study. The activation of *P53* genes often results in either cell-cycle arrest or apoptosis. *P53* protein is an important regulator which provokes a cellular response to various signals of stress (Hassin et al., 2023). This is attributed to its tumour suppressor role via persuading the growth arrest, apoptosis, and inhibition of angiogenesis. Thus, the low levels of *P53* potentiate cell-cycle arrest, whereas its higher level induces apoptosis (Borrero et al., 2021; Liebl et al., 2021). Apoptosis is controlled by the release of cytochrome C that is affected by either pro-apoptotic [Bcl-2-associated X protein (BAX)] or anti-apoptotic [B-cell lymphoma 2 (BCL2)] proteins (Qian et al., 2022; Kaloni et al., 2023). Investigation of the gene expressions using real-time PCR proved that compounds 3a, 3b, and 3e overexpressed *P53* and *BAX* and downregulated *BCL-2* expression. These findings established that compounds 3a, 3b, and 3e induced apoptosis in a *P53*-dependent manner (Ghatei et al., 2017; Lopez et al., 2022; Ismail et al., 2022). Our results demonstrated that compounds 3a, 3b, and 3e have exerted potential anticancer effect on the MDA-MB-231 breast cancer cells.

## 5. Conclusion

Twelve novel quinazoline derivatives (5a-l) having similar structural features with two known FDA-approved anticancer drugs, Ispinesib (KSP inhibitor) and Idelalisib (PI3K $\delta$ ) were designed, synthesized, and characterized. The molecular docking studies revealed that compounds 3a, 3b, 3e, 3g, 3h have strong binding affinity with KSP and PI3K $\delta$ . All these five compounds were found to be potent in nanomolar range in inhibiting KSP ATPase and PI3K $\delta$  activity. Compounds 3a, 3b, and 3e were found to have lowest IC<sub>50</sub> for MDA-MB-231 cells with values 14.51  $\mu$ M, 16.27  $\mu$ M, and 9.97  $\mu$ M, respectively, as compared to doxorubicin (1.41  $\mu$ M) in MTT assay. The compounds were found to be safe on normal oral epithelial cells. The flow cytometric analysis study revealed an increase in the early and late apoptotic cells. qRT-PCR study concluded that apoptosis was induced in a *P53*-dependant manner due to the upregulation of the *P53* and *BAX* genes in addition to the downregulation of the *BCL-2* gene. Further study is required to reveal the impact of the tested compounds (3a, 3b, and 3e) on other cancer cell types at molecular level.

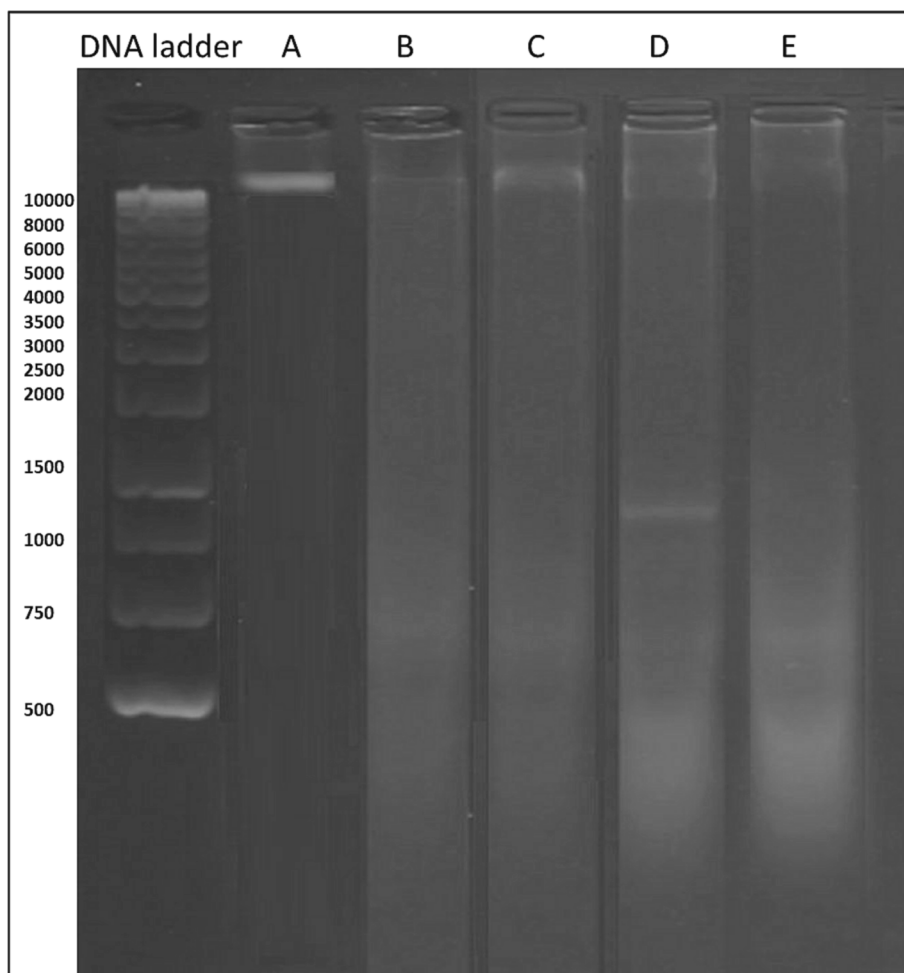


Fig. 14. DNA fragmentation of MDA-MB-231 by the tested compounds, where A is the untreated cells, B is compound 3a, C is compound 3b, D is compound 3e, and E is doxorubicin (standard drug).

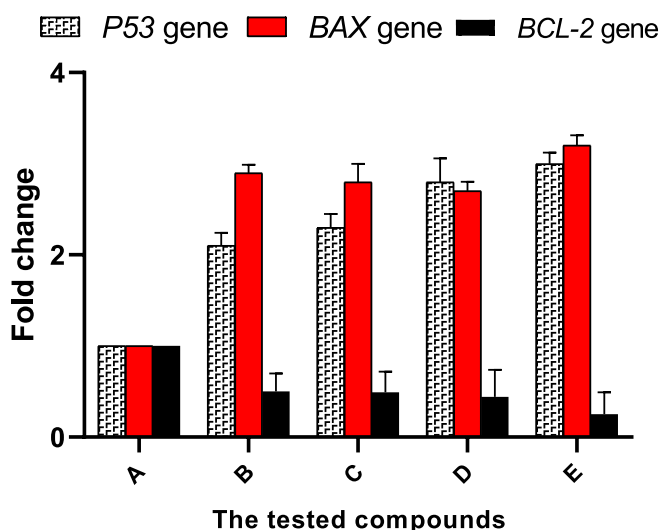


Fig. 15. Bar chart showing the effect of the compounds 3a (B), 3b (C), 3e (D), and doxorubicin (E) on the relative gene expression of P53, BAX, and BCL-2 genes, where (A) represents control (untreated cells).

### 6. Author’s contribution

All authors contributed significantly to the manuscript.

### CRediT authorship contribution statement

**Manal A. Alossaimi:** Conceptualization, Supervision, Writing – original draft. **Yassine Riadi:** Investigation, Methodology, Writing – review & editing. **Ghaida N. Alnuwaybit:** Visualization, Formal analysis. **Shadab Md:** Resources, Formal analysis, Project administration. **Huda Mohammed Alkreathy:** Resources, Validation. **Engy Elekhaway:** Investigation, Validation, Writing – review & editing. **Mohammed H. Geesi:** Validation, Formal analysis. **Safar M. Alqahtani:** Validation, Formal analysis, Methodology. **Obaid Afzal:** Data curation, Investigation, Software, Writing – review & editing.

### Funding

This research work was funded by Institutional Fund Projects under grant no. (IFPIP-1736-166-1443).

### Declaration of competing interest

The authors declare that they have no known competing financial interests or personal relationships that could have appeared to influence the work reported in this paper.

## Acknowledgement

This research work was funded by Institutional Fund Projects under grant no. (IFPIP-1736-166-1443). Therefore, the authors gratefully acknowledge technical and financial support from the Ministry of Education and King Abdulaziz University, DSR, Jeddah, Saudi Arabia.

## Appendix A. Supplementary data

Supplementary data to this article can be found online at <https://doi.org/10.1016/j.jsps.2024.101971>.

## References

- Alotaibi, B., Negm, W.A., Elekhawy, E., El-Masry, T.A., Elseady, W.S., Saleh, A., Alotaibi, K.N., El-Sherbeni, S.A., 2021. Antibacterial, immunomodulatory, and lung protective effects of boswelliadalzielii oleoresin ethanol extract in pulmonary diseases. *in vitro* and *in vivo* studies. *Antibiotics* 10 (12), 1444.
- Anand, U., Dey, A., Chandel, A.K.S., Sanyal, R., Mishra, A., Pandey, D.K., De Falco, V., Upadhyay, A., Kandimalla, R., Chaudhary, A., 2023. Cancer chemotherapy and beyond: current status, drug candidates, associated risks and progress in targeted therapeutics. *Genes & Diseases* 10 (4), 1367–1401.
- Aslam, M.S., Naveed, S., Ahmed, A., Abbas, Z., Gull, I., Athar, M.A., 2014. Side effects of chemotherapy in cancer patients and evaluation of patients opinion about starvation based differential chemotherapy. *Journal of Cancer Therapy*.
- Attallah, N.G., El-Sherbeni, S.A., El-Kadem, A.H., Elekhawy, E., El-Masry, T.A., Elmongy, E.I., Altwajry, N., Negm, W.A., 2022. elucidation of the metabolite profile of *Yucca gigantea* and assessment of its cytotoxic, antimicrobial, and anti-inflammatory activities. *Molecules* 27 (4), 1329.
- Ayala-Aguilera, C.C., Valero, T., Lorente-Macias, A., Baillache, D.J., Croke, S., Unciti-Broceta, A., 2021. Small molecule kinase inhibitor drugs (1995–2021): medical indication, pharmacology, and synthesis. *Journal of Medicinal Chemistry* 65 (2), 1047–1131.
- Borrero, L.J.H., El-Deiry, W.S., 2021. Tumor suppressor p53: Biology, signaling pathways, and therapeutic targeting. *Biochimica et Biophysica Acta (BBA)-Reviews on Cancer* 1876 (1), 188556.
- Chen, F., Zhuang, X., Lin, L., Yu, P., Wang, Y., Shi, Y., Hu, G., Sun, Y., 2015. New horizons in tumor microenvironment biology: challenges and opportunities. *BMC Medicine* 13 (1), 1–14.
- Debela, D.T., Muzazu, S.G., Heraro, K.D., Ndalama, M.T., Mesele, B.W., Haile, D.C., Kitui, S.K., Manyazewal, T., 2021. New approaches and procedures for cancer treatment: Current perspectives. *SAGE Open Medicine* 9, 20503121211034366.
- Elmore, S., 2007. Apoptosis: a review of programmed cell death. *Toxicologic Pathology* 35 (4), 495–516.
- Friesner, R.A., Murphy, R.B., Repasky, M.P., Frye, L.L., Greenwood, J.R., Halgren, T.A., Sanschagrin, P.C., Mainz, D.T., 2006. Extra precision glide: docking and scoring incorporating a model of hydrophobic enclosure for protein–ligand complexes. *J. Med. Chem.* 49 (21), 6177–6196.
- Funk, C.J., Davis, A.S., Hopkins, J.A., Middleton, K.M., 2004. Development of high-throughput screens for discovery of kinesin adenosine triphosphatase modulators. *Analytical Biochemistry* 329 (1), 68–76.
- Ghatei, N., Nabavi, A.S., Toosi, M.H.B., Azimian, H., Homayoun, M., Targhi, R.G., Haghiri, H., 2017. Evaluation of bax, bcl-2, p21 and p53 genes expression variations on cerebellum of BALB/c mice before and after birth under mobile phone radiation exposure. *Iranian Journal of Basic Medical Sciences* 20 (9), 1037.
- Hanahan, D., 2022. Hallmarks of cancer: new dimensions. *Cancer Discovery* 12 (1), 31–46.
- Hassin, O., Oren, M., 2023. Drugging p53 in cancer: one protein, many targets. *Nature Reviews Drug Discovery* 22 (2), 127–144.
- Ismail, Z., Dam, J., Penny, C., de Koning, C.B., Harmse, L., 2022. Copper-imidazo [1,2-a] pyridines differentially modulate pro-and anti-apoptotic protein and gene expression in HL-60 and K562 leukaemic cells to cause apoptotic cell death. *Biochimica et Biophysica Acta (BBA)-Molecular Cell Research* 1869 (1), 119160.
- Julian, L., Olson, M.F., 2015. Apoptotic membrane dynamics in health and disease. *Cell Health and Cytoskeleton* 133–142.
- Kaan, H.Y.K., Major, J., Tkocz, K., Kozielski, F., Rosenfeld, S.S., 2013. “Snapshots” of ispinesib-induced conformational changes in the mitotic kinesin Eg5. *Journal of Biological Chemistry* 288 (25), 18588–18598.
- Kaloni, D., Diepstraten, S.T., Strasser, A., Kelly, G.L., 2023. BCL-2 protein family: Attractive targets for cancer therapy. *Apoptosis* 28 (1–2), 20–38.
- Kumari, R., Jat, P., 2021. Mechanisms of cellular senescence: cell cycle arrest and senescence associated secretory phenotype. *Frontiers in Cell and Developmental Biology* 9, 485.
- Lannutti, B.J., Meadows, S.A., Herman, S.E., Kashishian, A., Steiner, B., Johnson, A.J., Byrd, J.C., Tyner, J.W., Loriaux, M.M., Deininger, M., Druker, B.J., 2011. CAL-101, a p110 $\delta$  selective phosphatidylinositol-3-kinase inhibitor for the treatment of B-cell malignancies, inhibits PI3K signaling and cellular viability. *Blood, the Journal of the American Society of Hematology* 117 (2), 591–594.
- Lee, S., Meng, X., Flatten, K., Loegering, D., Kaufmann, S., 2013. Phosphatidylserine exposure during apoptosis reflects bidirectional trafficking between plasma membrane and cytoplasm. *Cell Death & Differentiation* 20 (1), 64–76.
- Li, Z.H., Hu, P.H., Tu, J.H., Yu, N.S., 2016. Luminal B breast cancer: Patterns of recurrence and clinical outcome. *Oncotarget* 7, 65024–65033.
- Liebl, M.C., Hofmann, T.G., 2021. The role of p53 signaling in colorectal cancer. *Cancers* 13 (9), 2125.
- Liu, L., Shen, W., Zhu, Z., Lin, J., Fang, Q., Ruan, Y., Zhao, H., 2018. Combined inhibition of EGFR and c-ABL suppresses the growth of fulvestrant-resistant breast cancer cells through miR-375-autophagy axis. *Biochem. Biophys. Res. Commun.* 498, 559–565.
- Lopez, A., Reyna, D.E., Gitego, N., Kopp, F., Zhou, H., Miranda-Roman, M.A., Nordström, L.U., Narayanagari, S.-R., Chi, P., Vilar, E., 2022. Co-targeting of BAX and BCL-XL proteins broadly overcomes resistance to apoptosis in cancer. *Nature Communications* 13 (1), 1199.
- Lukasiewicz, S., Czezelewski, M., Forma, A., Baj, J., Sitarz, R., Stanislawek, A., 2021. Breast cancer—epidemiology, risk factors, classification, prognostic markers, and current treatment strategies—an updated review. *Cancers* 13 (17), 4287.
- Malongang, F., McGaw, L.J., Olaokun, O.O., Mudau, F.N., 2022. Anti-Inflammatory, Anti-Diabetic, Anti-Oxidant and Cytotoxicity Assays of South African Herbal Teas and Bush Tea Blends. *Foods* 11 (15), 2233.
- Murad, H., Hawat, M., Ekhtiar, A., AlJapawe, A., Abbas, A., Darwish, H., Sbenati, O., Ghannam, A., 2016. Induction of G1-phase cell cycle arrest and apoptosis pathway in MDA-MB-231 human breast cancer cells by sulfated polysaccharide extracted from *Laurencia papillosa*. *Cancer Cell International* 16 (1), 1–11.
- Navya, P., Kaphle, A., Srinivas, S., Bhargava, S.K., Rotello, V.M., Daima, H.K., 2019. Current trends and challenges in cancer management and therapy using designer nanomaterials. *Nano Convergence* 6 (1), 1–30.
- Noh, J.-I., Mun, S.-K., Lim, E.H., Kim, H., Chang, D.-J., Hur, J.-S., Yee, S.-T., 2021. Induction of apoptosis in MDA-MB-231 cells treated with the methanol extract of lichen *Physconia hokkaidensis*. *Journal of Fungi* 7 (3), 188.
- Poon, I.K., Lucas, C.D., Rossi, A.G., Ravichandran, K.S., 2014. Apoptotic cell clearance: basic biology and therapeutic potential. *Nature Reviews Immunology* 14 (3), 166–180.
- Purcell, J.W., Davis, J., Reddy, M., Martin, S., Samayoa, K., Vo, H., Thomsen, K., Bean, P., Kuo, W.L., Ziyad, S., Billig, J., 2010. Activity of the kinesin spindle protein inhibitor ispinesib (SB-715992) in models of breast cancer. *Clinical Cancer Research* 16 (2), 566–576.
- Qian, S., Wei, Z., Yang, W., Huang, J., Yang, Y., Wang, J., 2022. The role of BCL-2 family proteins in regulating apoptosis and cancer therapy. *Frontiers in Oncology* 12, 985363.
- Rahman, N.A., Yazan, L.S., Wibowo, A., Ahmat, N., Foo, J.B., Tor, Y.S., Yeap, S.K., Razali, Z.A., Ong, Y.S., Fakurazi, S., 2016. Induction of apoptosis and G 2/M arrest by amepelonsin E from *Dryobalanops* towards triple negative breast cancer cells, MDA-MB-231. *BMC Complementary and Alternative Medicine* 16, 1–9.
- Ramadan, M.A., Shawkey, A.E., Rabeh, M.A., Abdellatif, A.O., 2019. Expression of P53, BAX, and BCL-2 in human malignant melanoma and squamous cell carcinoma cells after tea tree oil treatment *in vitro*. *Cytotechnology* 71, 461–473.
- Samarghandian, S.; Shabestari, M.M. DNA fragmentation and apoptosis induced by saffranal in human prostate cancer cell line. *Indian journal of urology (IJU: journal of the Urological Society of India)*, 2013, 29(3), 177.
- Somoza, J.R., Koditek, D., Villaseñor, A.G., Novikov, N., Wong, M.H., Liclican, A., Xing, W., Lagpacan, L., Wang, R., Schultz, B.E., Papalia, G.A., 2015. Structural, biochemical, and biophysical characterization of idelalisib binding to phosphoinositide 3-kinase  $\delta$ . *Journal of Biological Chemistry* 290 (13), 8439–8446.
- Su, T.T., 2020. Non-apoptotic roles of apoptotic proteases: new tricks for an old dog. *Open Biology* 10 (8), 200130.
- Sung, H.; Ferlay, J.; Siegel, R. L.; Laversanne, M.; Soerjomataram, I.; Jemal, A.; Bray, F., Global cancer statistics 2020: GLOBOCAN estimates of incidence and mortality worldwide for 36 cancers in 185 countries. *CA: a cancer journal for clinicians*, 2021, 71(3), 209-249.
- Van Swearingen, A.E.D., Sambade, M.J., Siegel, M.B., Sud, S., McNeill, R.S., Bevilacqua, S.M., Chen, X., Bash, R.E., Mounsey, L., Golitz, B.T., et al., 2017. Combined kinase inhibitors of MEK1/2 and either PI3K or PDGFR are efficacious in intracranial triple-negative breast cancer. *Neuro Oncol.* 19, 1481–1493.
- Wang, Y.-L., Overstreet, A.-M., Chen, M.-S., Wang, J., Zhao, H.-J., Ho, P.-C., Smith, M., Wang, S.-C., 2015. Combined inhibition of EGFR and c-ABL suppresses the growth of triple-negative breast cancer growth through inhibition of HOTAIR. *Oncotarget* 6, 11150–11161.
- Webb, M.R., 1992. A continuous spectrophotometric assay for inorganic phosphate and for measuring phosphate release kinetics in biological systems. *Proc. Natl. Acad. Sci. USA* 89, 4884–4887.
- Zayed, M.F., 2023. Medicinal chemistry of quinazolines as anticancer agents targeting tyrosine kinases. *Scientia Pharmaceutica*. 91 (2), 18.
- Zhao, W., Qiu, Y., Kong, D., 2017. Class I phosphatidylinositol 3-kinase inhibitors for cancer therapy. *Acta Pharmaceutica Sinica B* 7 (1), 27–37.